Quasiclassical Trajectory Study of the Environmental Reaction $O + HO_2 \rightarrow OH + O_2$

W. Wang, R. González-Jonte, and A. J. C. Varandas*

Departamento de Química, Universidade de Coimbra, P-3049 Coimbra Codex, Portugal

Received: March 13, 1998; In Final Form: June 12, 1998

We report a detailed dynamics and kinetics study of the title reaction over the range of translational energies $0.418 \leq E_{tr}/\text{kJ mol}^{-1} \leq 62.760$ by employing the quasiclassical trajectory method and a recently reported double many-body expansion potential energy surface for ground-state HO_3. A comparison of the calculated thermal rate constants with the available experimental results is also presented.

I. Introduction

The reaction of a oxygen atom $O(^3P)$ with a hydroperoxyl radical $HO_2(^2A'')$ in their ground electronic states,

$$O + HO_2 \rightarrow OH + O_2 \quad (1)$$

is important in the chemistry of the mesosphere and upper stratosphere. In particular, reaction 1 provides a major odd-oxygen destruction pathway in these regions of the atmosphere and along with the reactions

$$O + OH \rightarrow H + O_2 \quad (2)$$

$$H + O_2 + M \rightarrow HO_2 + M \quad (3)$$

$$H + O_3 \rightarrow OH + O_2 \quad (4)$$

plays a major role in controlling the partitioning among H, OH, and HO_2 radicals in the upper stratosphere.[1] It is also a chain-breaking step in combustion processes.[2] Due to its importance as an environmental reaction (i.e., in atmospheric chemistry and combustion processes), several experimental studies have been reported in the literature.[3−7] In all cases, very large rate coefficients have been measured.

Two possible mechanisms for $OH + O_2$ formation have been suggested:[8] (i) direct H abstraction by the oxygen atom,

$$O + HO_2 \rightarrow O\cdots HO_2 \rightarrow OH + O_2 \quad (5)$$

and (ii) O abstraction via formation of a HO_3 complex,

$$O + HO_2 \rightarrow O\cdots O_2H \rightarrow OH + O_2 \quad (6)$$

The former involves a tight transition state, while the latter occurs on a purely attractive potential energy surface. Experimentally, the kinetic results led several authors[3,5,7] to suggest that the title reaction should follow the oxygen atom abstraction mechanism. Sridharan et al.[9] confirmed such a mechanism by carrying out an $^{16}O/^{18}O$ isotopic substitution experiment in which the products of the title reaction were monitored in a discharge flow system.

In this work, we report a detailed theoretical study of reaction 1 by using the quasiclassical trajectory (QCT) method and a recently reported single-valued double many-body expansion (DMBE) potential energy surface for the electronic ground state of HO_3. In addition to investigate theoretically the mechanism of the title reaction, we provide a comparison of calculated thermal rate coefficients with the available experimental results. The paper is organized as follow. Section II provides a brief survey of the $HO_3(^2A)$ DMBE potential energy surface, while the computational method is surveyed in section III. The results and discussion are presented in section IV. Section V gathers the major conclusions.

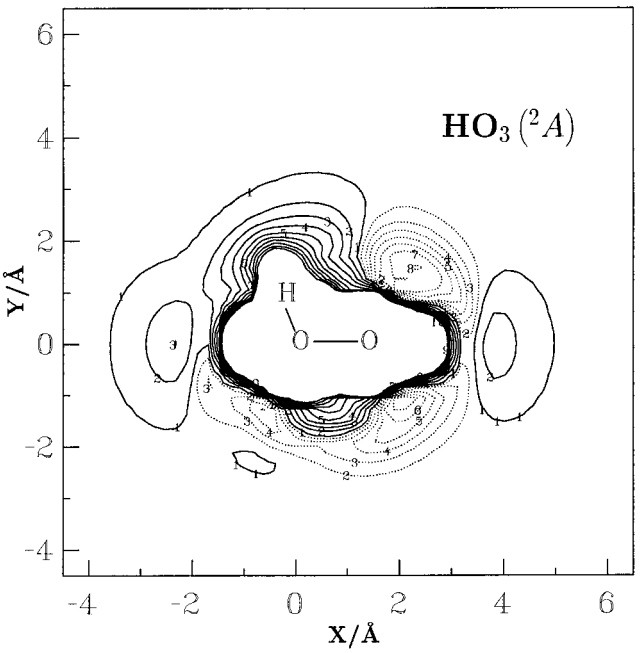

Figure 1. Isoenergy contour plot for a oxygen atom moving coplanarly around a partially relaxed HO_2 radical ($0.8650 \leq R_{OH}/\text{Å} \leq 1.0767$, $1.1189 \leq R_{OO}/\text{Å} \leq 1.5422$, $94.3 \leq \angle\text{HOO/deg} \leq 114.3$). The solid contours start at -732.515 kJ mol^{-1} (which corresponds to the $O + HO_2$ dissociation limit) and are equally spaced by 52.510 kJ mol^{-1}. The dotted contours start also at -732.515 kJ mol^{-1} but are equally spaced by -26.255 kJ mol^{-1}.

II. Potential Energy Surface

In this work we have used the six-dimensional (6D) DMBE potential energy surface[10] for ground-state HO_3, which has been previously employed[11,12] to study reaction 4 with good results. Since it has been described in detail elsewhere,[10] we focus here on its main topographical features which are of relevance for the title reaction.

Figure 1 shows a contour plot of the DMBE potential energy surface for an oxygen atom moving coplanarly around a partially

S1089-5639(98)01495-9 CCC: $15.00
Published on Web 08/07/1998

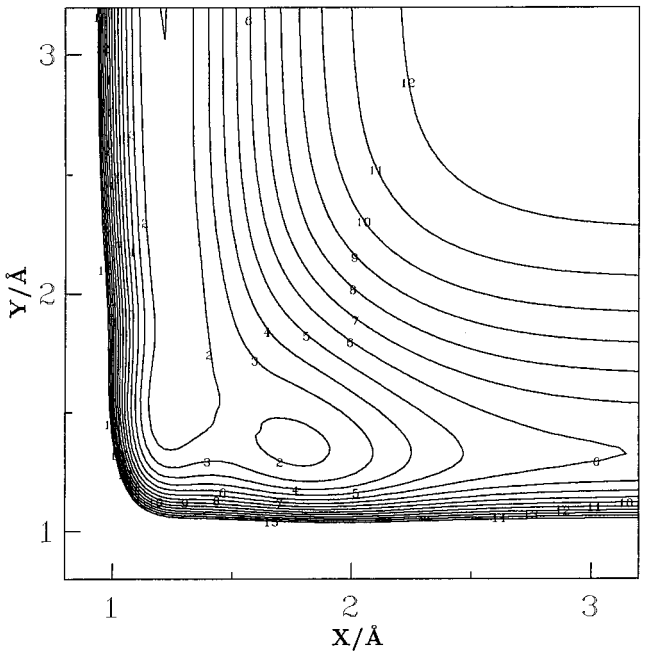

Figure 2. Isoenergy contour plot for the reaction $O + HO_2 \rightarrow OH + O_2$ via an oxygen atom abstraction mechanism. The *x*-axis represents the distance between the incoming oxygen atom and the terminal oxygen atom, while the *y*-axis denotes the O−O distance in the HO_2 radical. The ∠OOO and ∠HOO angles as well as the torsion angle ∠HOOO and the H−O distance are partially relaxed ($112.7 \leq \theta_{OOO}$/deg ≤ 118.7, $94.6 \leq \theta_{HOO}$/deg ≤ 104.3, $82.6 \leq \phi_{HOOO}$/deg ≤ 90.6, $0.9708 \leq R_{OH}$/Å ≤ 1.0315). Contours start at −949.827 kJ mol^{-1} (which corresponds to the $OH + O_2$ dissociation limit) and are equally spaced by 41.840 kJ mol^{-1}.

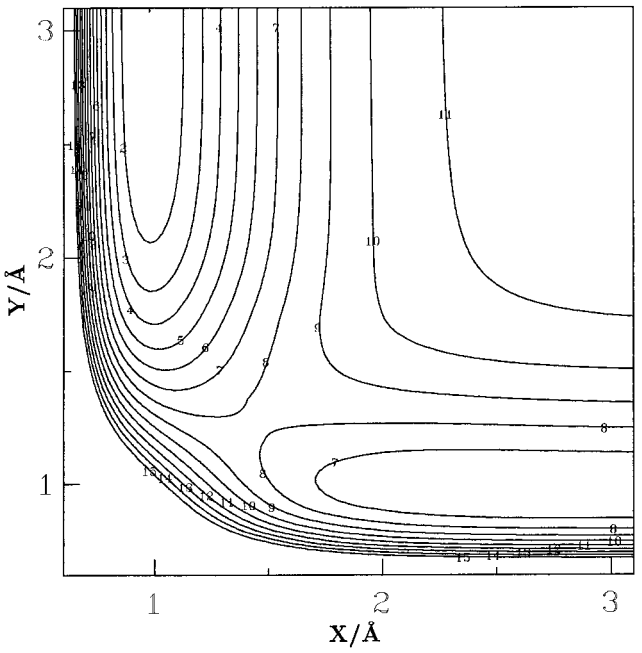

Figure 3. Isoenergy contour plot for the reaction $O + HO_2 \rightarrow OH + O_2$ via a hydrogen atom abstraction mechanism. The *x*-axis represents the distance between the incoming oxygen atom and the hydrogen atom, while the *y*-axis denotes the O−H distance in the HO_2 radical. The ∠OHO and ∠HOO angles as well as the O−O bond distance are partially relaxed ($170 \leq \theta_{OHO}$/deg ≤ 180, $100 \leq \theta_{HOO}$/deg ≤ 110, $1.2075 \leq R_{OO}$/Å ≤ 1.3306). The contours start at −949.827 kJ mol^{-1} (the $OH + O_2$ dissociation limit) and are equally spaced by 41.840 kJ mol^{-1}.

relaxed HO_2 radical. Note that the middle oxygen atom of HO_2 is fixed at the origin and that the O−H and O−O bond distances as well as the ∠HOO angle have been partially relaxed ($0.8650 \leq R_{OH}$/Å ≤ 1.0767, $1.1189 \leq R_{OO}$/Å ≤ 1.5422, $94.3 \leq \theta_{HOO}$/deg ≤ 114.3). We observe two minima associated with the terminal oxygen atom of the HO_2 radical and one in the vicinity of its central oxygen atom. The potential energy surface is also seen to be purely attractive for O approaching the terminal oxygen atom through a nonlinear geometry.

In Figure 2, we show a contour plot of the title reaction for the regions of configurational space with relevance in the oxygen atom abstraction mechanism (see eq 6). The *x*-axis represents now the distance between the incoming oxygen atom and the terminal oxygen atom of HO_2, while the *y*-axis denotes the O−O distance in the HO_2 radical. The ∠OOO, ∠HOO, and ∠HOOO torsion angles as well as the H−O distance have been partially relaxed ($112.7 \leq \theta_{OOO}$/deg ≤ 118.7, $94.6 \leq \theta_{OO}$/deg ≤ 104.3, $82.6 \leq \phi_{HOOO}$/deg ≤ 90.6, $0.9708 \leq R_{OH}$/Å ≤ 1.0315, respectively) in obtaining Figure 2. It is clear that no barrier is present along the minimum energy path. This observation agrees with Dupuis et al.,[13] who have found no barrier along the reaction path in their ab initio electronic struture calculations. It should be noted that the classical exothermicity of the title reaction in the HO_3 DMBE potential energy surface is ca. 218 kJ mol^{-1}, a value that is in agreement with the corresponding experimental result.

As it has already been pointed out, the hydrogen atom abstraction reaction path is expected to have a tight transition state.[8] Figure 3 shows energy contours for the oxygen atom attacking the hydrogen atom in the plane of the HO_2 radical. The *x*-axis represents here the distance between the incoming oxygen atom and the hydrogen atom, while the *y*-axis stands for the O−H bond distance in the HO_2 radical. As before, the angles ∠OHO and ∠HOO as well as the O−O distance have been allowed to partially relax ($170 \leq \theta_{OHO}$/deg ≤ 180, $100 \leq \theta_{HOO}$/deg ≤ 110, $1.2075 \leq R_{OO}$/Å ≤ 1.3306) to obtain Figure 3. Clearly, there is a transition state on the reaction path, with the potential barrier being about 75 kJ mol^{-1} above the energy of the $O + HO_2$ reactants, a value that is slightly larger than that predicted from the ab initio results of Dupuis et al.[13] In fact, from their CI(DZP) calculations for a geometry similar to the saddle point in Figure 3, the authors have found[13] the transition state to be 60 kJ mol^{-1} above the energy of $O + HO_2$.

III. Computational Method

To run the classical trajectories, we have used an extensively adapted version of the MERCURY[14] code which accommodates the HO_3 DMBE potential energy surface and makes the appropriate assignment of all reactive channels. Calculations have been carried for atom−triatom translational energies in the range $0.418 \leq E_{tr}$/kJ mol^{-1} ≤ 62.760, as specified in Table 1. In all calculations, the HO_2 radical has been kept in its ground vibrational state. A fixed normal mode energy sampling has been adopted. The initial normal mode coordinates and their time derivatives have been obtained following the standard procedure[14] as

$$Q_i = A_i \cos(2\pi\xi_i) \tag{7}$$

$$\dot{Q}_i = -\omega_i A_i \sin(2\pi\xi_i) \tag{8}$$

where A_i and ω_i are the amplitude and frequency (respectively) of the *i*th normal mode, and ξ_i is a pseudorandom number ranging from zero to unity which has been chosen to sample its vibrational phase ($2\pi\xi_i$). For every value of E_{tr}, the rotational

TABLE 1: Summary of the Trajectory Calculations.[a] All Symbols Have Meaning Assigned in the Text

E_{tr} (kJ mol^{-1})	b_{max} (Å)	OH + O_2 formation				exchange reaction			
		N_r	P_r	σ^r/Å^2	$\Delta\sigma^r$/Å^2	N_r	P_r	σ^r/Å^2	$\Delta\sigma^r$/Å^2
0.418	8.25	434	0.868	185.60	3.24	2	0.004	0.86	0.60
2.092	6.25	408	0.816	100.14	2.13	4	0.008	0.98	0.49
4.184	5.50	3486	0.697	66.26	0.62	30	0.006	0.57	0.10
8.368	5.00	325	0.750	51.05	1.68	5	0.010	0.78	0.35
20.920	4.25	333	0.666	37.79	1.20	7	0.014	0.79	0.30
41.840	4.00	305	0.610	30.66	1.10	12	0.024	1.21	0.35
62.760	4.00	252	0.504	25.33	1.12	14	0.028	1.41	0.37

[a] For the initial translational energy $E_{tr} = 4.184$ kJ mol^{-1}, $N = 5000$, while for the other initial translational energies $N = 500$.

energy about each principal axis of inertia of HO_2 has been taken as $k_BT/2$, while the rotational temperature has been assumed to be 300 K. This corresponds to an intermediate value in the range of temperatures $100 \leq T/K \leq 500$, over which most of the thermal rate coefficients have been reported. Also following the current practice, the orientation of the molecular rotation has been specified randomly. In turn, the atom−triatom initial separation has been fixed at 15 Å, a value that is sufficiently large to warrant that the interaction energy between the oxygen atom and the HO_2 radical is negligible. All other initial conditions have been sampled using the standard procedure.[14]

The integration of the classical equations of motion has been carried out by means of a combined fourth-order Runge−Kutta and fifth-order Adams−Moulton algorithm. The integration time step size has been fixed at $\Delta t = 2.5 \times 10^{-16}$ s such that the total energy could be conserved to better than 2 parts in 10^3. The final state analysis of the products has been carried out using the standard procedure.[14]

Batches of 50 trajectories per collisional energy have been first run to determine the maximum value of the impact parameter (b_{max}) which leads to the title reaction. Batches of 500 trajectories have then been carried out for each of the seven translational energies reported in Table 1, except for $E_{tr} = 4.184$ kJ mol^{-1}, for which we have carried out a batch of trajectories 10 times larger. This is sufficient to warrant an error in the cross section of typically a few percent. Table 1 summarizes the calculated values of b_{max} and the results obtained from the trajectory calculations.

For a specified translational energy, the reactive cross section can be calculated by

$$\sigma^r = \pi b_{max}^2 P_r \tag{9}$$

with the associated 68% error limit being given by

$$\Delta\sigma^r = \left[\frac{N - N_r}{NN_r}\right]^{1/2} \sigma^r \tag{10}$$

where N_r is the number of reactive trajectories in a total of N, $P_r = N_r/N$ is the reactive probability, and the maximum impact parameter b_{max} that leads to reaction is a function of the translational energy.

From the total reactive cross section and assuming a Maxwell−Boltzmann distribution over the translational energy, the thermal rate constant has been calculated as

$$k(T) = f(T)\left(\frac{2}{k_BT}\right)^{3/2}\left(\frac{1}{\pi\mu}\right)^{1/2}\int_0^\infty E_{tr}\sigma^r \exp(-E_{tr}/k_BT)\, dE_{tr} \tag{11}$$

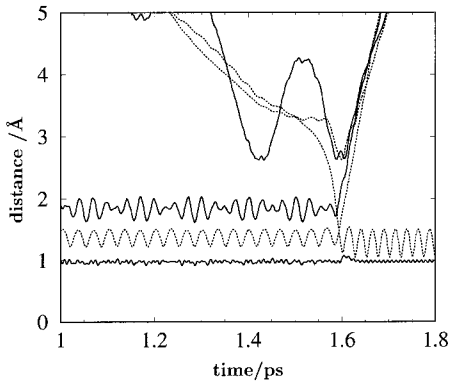

Figure 4. Trajectory for the reaction $O + HO_2 \rightarrow OH + O_2$ at $E_{tr} = 4.184$ kJ mol^{-1}. The solid lines refer to the O−H distances, while the dashed lines refer to the O−O distances.

where μ is the reduced mass of the atom−triatom colliding pair, and $f(T)$ is the appropriate electronic degeneracy factor (see section IV).

IV. Results and Discussion

Table 1 provides a summary of the trajectory calculations reported in the present work. They involve a total of about 8×10^3 trajectories for the seven specified initial translational energies. For these initial translational energies, the only opened reactive channels are the following:

$$O_c + HO_aO_b \rightarrow O_b + HO_aO_c \tag{12}$$

$$O_c + HO_aO_b \rightarrow O_aH + O_bO_c \tag{13}$$

$$O_c + HO_aO_b \rightarrow O_cH + O_aO_b \tag{14}$$

where the indices *a*, *b*, and *c* label the three different oxygen atoms. Clearly, reaction 12 corresponds to the oxygen atom exchange reaction, while reaction 13 refers to the formation of $OH + O_2$ products via the oxygen atom abstraction mechanism. Of course, reaction 14 refers to the hydrogen atom abstraction.

Our first observation from Table 1 is that for all trajectories calculated in the present work none lead to reaction 14. This means that, for the DMBE potential energy surface used in the present work, the title reaction occurs only via the oxygen atom abstraction path. Such a result is consistent with the experimental finding of Sridharan et al.[9] Thus, the results reported in Table 1 for $OH + O_2$ formation refer only to reaction 13 and hence show that the collisions between the oxygen atom and the HO_2 radical lead mainly to formation of such products. In fact, the exchange reaction has very low probability of occurrence, with the corresponding reactive cross section being essentially negligible.

A. Dynamical Details. Figure 4 illustrates a reactive trajectory for the reaction $O + HO_2 \rightarrow OH + O_2$ at the initial translational energy $E_{tr} = 4.184$ kJ mol^{-1}. It is seen that the lifetime of the HO_3 intermediate is typically very short (≤0.2 ps), with the energy being released mostly as vibrational energy of the O_2 molecule and translational energy. In this trajectory the reaction follows the oxygen abstraction mechanism: the incoming oxygen atom attacks the terminal oxygen atom of the HO_2 radical to form the nascent O_2 molecule, with the remaining OH fragment acting basically as a spectator during the collisional event. This reactive pathway is consistent with the topographical features of the potential energy surface which has been discussed in section II.

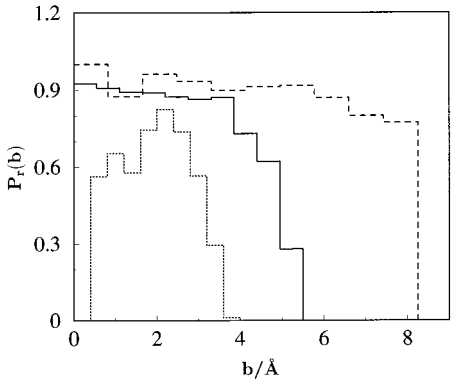

Figure 5. Opacity function for the reaction $O + HO_2 \rightarrow OH + O_2$: dashed line, $E_{tr} = 0.418$ kJ mol^{-1}; solid line, $E_{tr} = 4.184$ kJ mol^{-1}; dotted line, $E_{tr} = 62.760$ kJ mol^{-1}.

Figure 5 shows the opacity function (i.e., reactive probability versus impact parameter) for the title reaction at three different collisional energies, $E_{tr} = 0.418$, 4.184, and 62.760 kJ mol^{-1}. It is clear that the maximum impact parameter that leads to reaction is largest for the lowest value of the initial translational energy. This result is consistent with the fact that the reaction takes place on a barrier-free potential energy surface where long-range forces play a major role. For $E_{tr} = 0.418$ kJ mol^{-1}, the reactivity is maintained near its maximum for all values of b, while for an energy 10 times larger ($E_{tr} = 4.184$ kJ mol^{-1}) the reactivity decreases smoothly with increasing value of the impact parameter. These observations may be rationalized from the fact that the centrifugal barrier for reaction results from a subtle balance of the long-range forces and the centrifugal energy, being related to the orbital angular momentum through the form

$$L = (2\mu E_{tr})^{1/2} b \qquad (15)$$

where μ is the reduced mass of the atom−triatom colliding pair, and b the impact parameter for the specific collision leading to reaction. Thus, for a fixed translational energy, an increase of b leads to an increase of the centrifugal barrier and hence to a decrease in the reaction probability. However, because the reaction is very exothermic, no long-lived trajectories are observed even for low collisional energies. For $E_{tr} = 62.760$ kJ mol^{-1}, the reaction probability is low both at small and large values of b, with the maximum of the opacity function (i.e., reactivity versus translational energy) occurring at $b \sim 2.4$ Å. From the potential energy surface features (see Figure 1), it is seen that, for the reaction to happen, the oxygen atom must attack the HO_2 radical through some favorable orientation. Of course, for low translational energies, the collision pair has enough time to be reoriented by the long-range forces to follow the minimum energy path. However, for high translational energies (e.g., $E_{tr} = 62.760$ kJ mol^{-1}), the collision occurs so quickly that there is not enough time for reorientation of the colliding pair to take place. This may explain why the reaction probability is low for small values of b.

The differential cross sections (divided by πb_{max}^2) are shown in Figure 6. The scattering angle, θ_{scatt}, is defined here as the angle between the velocity vectors $\vec{v}_{O_2} - \vec{v}_{OH}$ and $\vec{v}_O - \vec{v}_{HO_2}$, with the zero of θ_{scatt} corresponding to forward scattering of the O_2 molecule with respect to the incoming oxygen atom. The average scattering angles ($\langle\theta_{scatt}\rangle$) for $E_{tr} = 0.418$, 4.184, and 62.760 kJ mol^{-1} are respectively 82.5°, 75.4°, and 62.9°. It is seen that the reaction is of stripping type, with the incoming oxygen atom pulling off the terminal oxygen atom in a forward direction. The average scattering angles are also found to

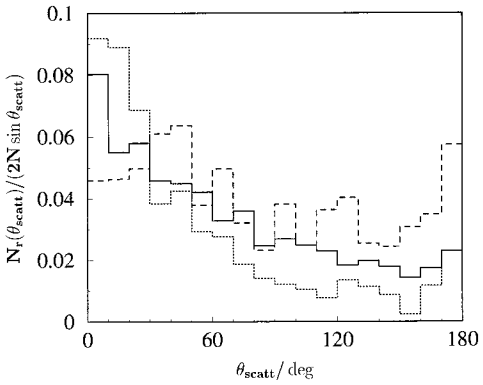

Figure 6. Differential cross section (divided by πb_{max}^2) for the reaction $O + HO_2 \rightarrow OH + O_2$: dashed line, $E_{tr} = 0.418$ kJ mol^{-1}; solid line, $E_{tr} = 4.184$ kJ mol^{-1}; dotted line, $E_{tr} = 62.760$ kJ mol^{-1}.

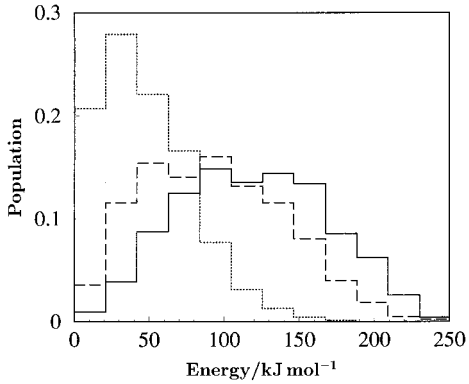

Figure 7. Energy distribution in the products for the reaction $O + HO_2 \rightarrow OH + O_2$ at $E_{tr} = 4.184$ kJ mol^{-1}. The dashed line represents the translational energy distribution, the solid line the internal energy distribution of the O_2, and the dotted line the internal energy distribution of the OH.

TABLE 2: Percentages of Energy Partitioned to Different Degrees of Freedom for the Reaction $O + HO_2 \rightarrow OH + O_2$ at $E_{tr} = 4.184$ kJ mol^{-1}

$\langle f_{vib}^{O_2}\rangle$	$\langle f_{rot}^{O_2}\rangle$	$\langle f_{vib}^{OH}\rangle$	$\langle f_{rot}^{OH}\rangle$	$\langle f_{trans}\rangle$
32.10	13.98	7.80	10.35	35.77

decrease with increasing collisional energy. This fact is consistent with the very short lifetimes of the HO_3 intermediate during the reaction. In summary, the oxygen atom abstraction occurs via a rapid O−O bond-breaking/bond-forming process.

B. Energy Distribution in the Products. In this section we analyze the energy distribution in the products by considering the specific case of $E_{tr} = 4.184$ kJ mol^{-1}, which is close to the average value of the translational energy for $T = 300$ K according to a Maxwell−Boltzmann distribution. To get good relative populations, a batch of 5000 trajectories has been run for this initial translational energy.

Figure 7 shows the energy distribution in the products of the title reaction for $E_{tr} = 4.184$ kJ mol^{-1}. Clearly, the maximum of the internal energy distribution for the OH radical occurs at a very low value. Conversely, most of the O_2 molecules have high internal energy. A study of the partitioning of the energy released in the product molecules is shown in Table 2. As expected from the analysis in Figure 7, we find that the released energy enters mainly into relative translational energy of HO with respect to O_2 and internal energy of the O_2 molecules.

Figure 8 shows the vibrational quantum number distributions for the OH and O_2 product diatomics. Clearly, they follow rather distinct patterns, with the vibrational distribution of OH

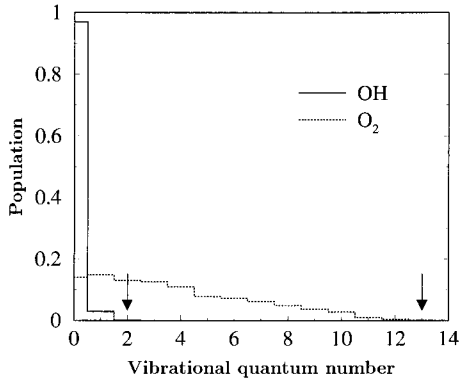

Figure 8. Histogram of the products vibrational state distributions for the reaction O + HO_2 → OH + O_2. The solid line stands for OH, and the dotted one for O_2. The errors indicate the maximum populated quantum numbers.

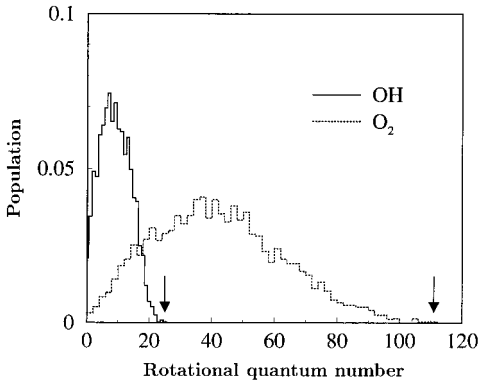

Figure 9. As in Figure 8 but for the rotational quantum numbers.

being considerably cooler than that of O_2 (the majority of the OH radicals are found to be in the ground vibrational state). In fact, the O_2 molecules are formed vibrationally hot, with the maximum populated vibrational quantum number being as large as $v = 13$. Note that from $v = 0$ to $v = 4$, the O_2 vibrational population distribution is more or less constant, and even shows a tendency for an inverted population peaking at $v = 1$. Thus, the title reaction provides a source of vibrationally hot O_2 molecules, which may have implications for the ozone chemistry in the stratosphere and mesosphere (ref 15, and references therein).

In Figure 9 we show the rotational distributions of OH and O_2. It is seen that the O_2 molecules can be populated at higher rotational quantum numbers than the OH radical, although the rotational energy distributions of OH and O_2 show rather similar patterns when plotted as a function of the rotational energy. Regarding the rotational state distributions in Figure 9, we note that the ground electronic state of OH($^2\Pi$) belongs to Hund's[16] case a or b or a mixture of the two. For a fast rotating OH, case b is expected to dominate, and hence the rotational quantum number is given by $j = 1, 2, ...$, with the smallest value being $j = \Lambda = 1$; Λ is the associated electronic angular momentum. For convenience, we use in the the present work the traditional boxing scheme which is appropriate to diatomic molecules in $^1\Sigma$ states and hence allows for values of the OH rotational quantum number equal to zero. A similar difficulty is encountered for O_2; this is a case b molecule for which only odd-numbered rotational states are allowed by symmetry, since the oxygen atoms have zero spin and the ground state is an antisymmetric $^3\Sigma_g^-$ electronic state. Thus, the problem has a quantum mechanical origin in both cases and is difficult to fix rigorously in the usual quasiclassical treatment of the dynamics,

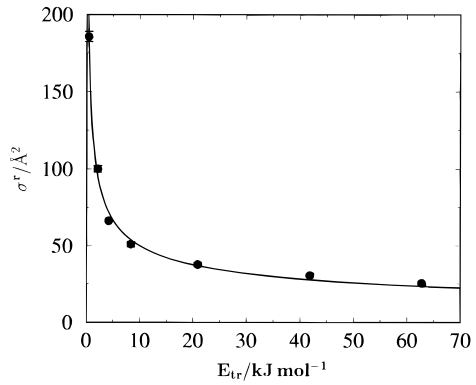

Figure 10. Reactive cross section σ_r as function of the initial translational energy for the reaction O + HO_2 → OH + O_2. Also indicated are the 68% error bars and, by the solid lines, the fitted curve given by eq 16.

although approximate schemes have been proposed by Luntz and Andresen,[17] Clary et al.,[18] and Varandas.[19] Since the limitations of the traditional approach are not expected to drastically alter the major trends of our results, we follow previous work[11] and use it also here. Thus, we simply round off the j quantum numbers of O_2 in such a way that only odd values are obtained (i.e., values between $j = 0$ and $j = 2$ are assigned to $j = 1$, and so on). For OH, we follow the traditional scheme and allow j to vary from $j = 0$ onward. As seen from Figure 9, the peaks arise in the vicinity of $j = 7$ for OH and $j = 37$ for O_2, while the maximum populated rotational quantum numbers can be as high as $j = 25$ for OH and $j = 111$ for O_2. From these distributions, the calculated average rotational energies (percentages) have been found to be 83.71 kJ mol^{-1} (10.35%) and 93.24 kJ mol^{-1} (13.98%) for OH and O_2 molecules, respectively. Unfortunately, no experimental results are available for the title reaction which might allow a test of our predictions.

C. Cross Sections and Thermal Rate Coefficient. Figure 10 shows the calculated reactive cross sections (σ^r) and the associated 68% error bars for formation of OH + O_2. We observe a marked decrease of the reactive cross sections with increasing value of the initial translational energy. Such dependence of the reactive cross sections is well described by the form

$$\sigma^r(E_{tr}) = n\pi(n-2)^{(2-n)/n}\left(\frac{C_n}{2E_{tr}}\right)^{2/n} \qquad (16)$$

where n and C_n are parameters to be determined from a least-squares fitting procedure. The optimum numerical values of these parameters have been found to be $n = 4.848$ and $C_n = 1595.204$. The units of these parameters are such that, with the translational energy in kJ mol^{-1}, the units of the cross section are Å^2. The fitted curve is also indicated in Figure 10 by the smooth solid line. Note that eq 16 is the form obtained from simple classical capture theory by considering the reactant species structureless and interacting through the long-range attractive potential

$$V = -C_n r^{-n} \qquad (17)$$

where C_n is the long-range coefficient for the atom−triatom interaction, and r is the distance between the atom and the center of mass of the triatomic molecule.[20,21]

By substituting eq 16 in eq 11 and performing the integration analytically, the thermal rate coefficient $k(T)$ assumes the form[22]

$$k(T) = f(T)\frac{2^{(3n-4)/2n} n\pi^{1/2}}{(n-2)^{n-2/n}\mu^{1/2}}\Gamma\left(\frac{2n-2}{n}\right)(k_B T)^{n-4/2n} C n^{2/n} \tag{18}$$

where $\Gamma[(2n-2)/n]$ is the gamma function, and μ is the reduced mass of the atom−triatom colliding pair. For the reaction $O + HO_2 \rightarrow OH + O_2$, the electronic degeneracy factor $f(T)$ is given by

$$f(T) = \frac{1}{5 + 3\exp\left(-\frac{227.6}{T}\right) + \exp\left(-\frac{325.9}{T}\right)} \tag{19}$$

which accounts in the usual way for the electronic degeneracies of $O(^3P) + HO_2(^2A'')$ and the fact that the DMBE potential energy surface refers to $HO_3(^2A)$.[10,23,24]

Figure 11 shows the thermal rate constant calculated using eq 18 for the temperature range 100−1700 K. Note that the calculations have been based on an average rotational temperature of 300 K, although we believe that this assumption does not drastically influence the accuracy of the final results for the extreme temperatures in the above range. Also included for comparison in Figure 11 are the available experimental results which have been reported in the literature.[3−6,25−29] Of these, the only studies that investigated the temperature dependence of the rate constant of reaction 1 are the pulsed laser photolysis results of Nicovich and Wine[7] for 266−391 K and the discharge flow measurements of Keyser[4] for 299−372 K. The others are measurements of the rate constant at 298,[3,5,6] 1050,[25] and 1600 K[26] which employ various techniques. In addition, panel a of Figure 11 shows the recommended rate constant[30] for the temperature range 200−400 K. It is seen that the calculated $k(T)$ follows a general pattern for the temperature dependence similar to that of the experimental results, although showing a smaller decrease with temperature than the recommended curve in the low-temperature regime. However, if we consider the complete set of experimental data (which includes the two points at 1050 and 1600 K), then one wonders whether the rate constant is expected to slightly increase with temperature at higher temperatures. Speculatively, one could attribute such an increase in the rate constant to the opening of a new reactive channel which could not be accounted for by the adiabatic dynamics calculations carried out in the present work using the single-valued HO_3 DMBE potential energy surface.[10] On the other hand, we have no access to the work of Peeters and Mahnen[25] and Day et al.[26] and hence cannot be not aware of the error bars associated with their data. Since our predicted values agree generally well with the high-temperature data, we tend to believe that the slope of the recommended rate law[30] may be slightly too exaggerated. If a smaller value is considered for ΔE in the Atkinson et al.[30] expression, then a closer agreement between theory and experiment can be globally reached. In this case, a smooth but somewhat flatter decaying curve is obtained, which is typical for reactions occurring on barrier-free potential energy surfaces such as that used in the present work for ground-state HO_3. In summary, we expect our calculated rate constant to reflect the general trends of the available experimental data, although perhaps too large by a factor of 30% or so depending on the specific value of the temperature being considered. This overestimation may be attributed both to innaccuracies of the potential energy surface and to the fact that the dynamics has been carried out classically. For example, no account is given of zero-point energy leakage, which frequently tends to overestimate the computed reactivity (ref 31, and references therein).

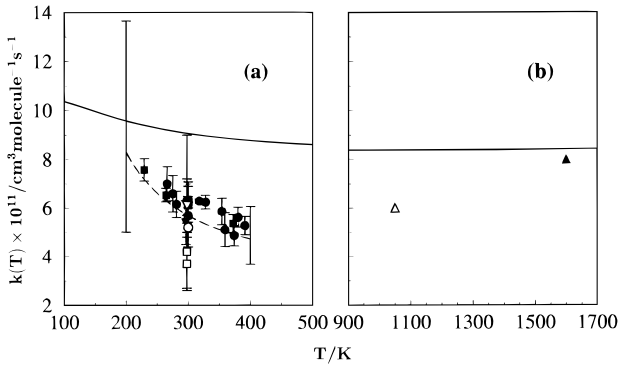

Figure 11. Thermal rate coefficients for the reaction $O + HO_2 \rightarrow OH + O_2$. The solid line indicates our results, while the dashed line represents the recommended experimental correlation[30] with the error bar at $T = 200$ and 400 K. Symbols: ○, ref 7; ■, ref 4; □, ref 28; ▽, ref 5; ▼, ref 3; ●, ref 6; *, ref 29; ▲, ref 25; △, ref 26.

V. Conclusions

We have carried out a quasiclassical trajectory study of the title reaction using a recently reported DMBE potential energy surface for the ground electronic state of HO_3. The calculated thermal rate coefficients are found to overestimate the recommended experimental results over the temperature range $200 \leq T/K \leq 400$ by a factor of up to 1.5 or so at 400 K, although showing general good agreement with experiment when the measured data for higher temperatures is also included. Thus, together with the work previously reported for the reaction $H + O_3 \rightarrow OH + O_2$, the present study provides evidence of the reliability of the $HO_3(^2A)$ DMBE potential energy surface reported elsewhere.[10] The calculations of the present work have also shown that the title reaction occurs exclusively via oxygen atom abstraction following a capture-type mechanism in which long-range forces are expected to play an important role at low energies. Such an abstraction reaction occurs via rapid breaking and formation of the O−O bonds, and hence the lifetime of the HO_3 intermediate is rather short. The excess energy of the reaction has been found to be released mainly as translational and internal energy of the O_2 molecule. In conclusion, because the title reaction has important implications in modeling the stratospheric ozone concentration, further experimental measurements would be welcome especially for temperatures higher than 400 K. These might shed some light on the validity of the correction suggested above for the dependence of the rate constant on temperature.

Acknowledgment. This work has the support of Fundação para a Ciência e Tecnologia, Portugal, under programmes PRAXIS XXI and FEDER (Contract 2/2.1/QUI/408/94).

References and Notes

(1) Crutzen, P. *Science* **1997**, *277*, 1951.
(2) Steinfeld, J. I.; Francisco, J. S.; Hase, W. L. *Chemical Kinetics and Dynamics*; Prentice Hall: Englewood Cliffs, NJ, 1989.
(3) Sridharan, U. C.; Qiu, L. X.; Kauman, F. *J. Phys. Chem.* **1982**, *86*, 4469.
(4) Keyser, L. F. *J. Phys. Chem.* **1982**, *86*, 3439.
(5) Ravishankara, A. R.; Wine, P. H.; Nicovich, B. M. *J. Chem. Phys.* **1983**, *78*, 6629.
(6) Brune, W. H.; Schwab, J. J.; Anderson, J. G. *J. Phys. Chem.* **1983**, *87*, 4503.
(7) Nicovich, J. M.; Wine, P. H. *J. Phys. Chem.* **1987**, *91*, 5118.
(8) Weisman, M.; Shum, L. S. G.; Heneghan, S. P.; Benson, S. W. *J. Phys. Chem.* **1981**, *85*, 2863.
(9) Sridharan, U. C.; Klein, F. S.; Kaufman, F. *J. Chem. Phys.* **1985**, *82*, 592.
(10) Varandas, A. J. C.; Yu, H. G. *Mol. Phys.* **1997**, *91*, 301.

(11) Yu, H. G.; Varandas, A. J. C. *J. Chem. Soc., Faraday Trans.* **1997**, *93*, 2651.

(12) Szichman, H.; Baer, M.; Varandas, A. J. C. *J. Phys. Chem.* **1997**, *101*, 8817.

(13) Dupuis, M.; Fitzgerald, G.; Hammond, B.; Lester, W. A., Jr.; Schaefer, H. F., III. *J. Chem. Phys.* **1986**, *84*, 2691.

(14) Hase, W. L. *MERCURY*: a general Monte-Carlo classical trajectory computer program, QCPE#453. An updated version of this code is *VENUS96*: Hase, W. L.; Duchovic, R. J.; Hu, X.; Komorniki, A.; Lim, K. F.; Lu, D.-H.; Peslherbe, G. H.; Swamy, K. N.; van de Linde, S. R.; Varandas, A. J. C.; Wang, H.; Wolf, R. J. *QCPE Bull.* **1996**, 16, 43.

(15) Varandas, A. J. C.; Wang, W. *Chem. Phys.* **1997**, *215*, 167.

(16) Herzberg, G. *Molecular Spectra and Molecular Structure. I. Spectra of Diatomic Molecules*; van Nostrand: New York, 1950.

(17) Luntz, A. C.; Andresen, P. *J. Chem. Phys.* **1980**, *72*, 5851.

(18) Clary, D. C.; Connor, J. N. L.; Southall, W. J. E. *J. Chem. Phys.* **1986**, *84*, 2620.

(19) Varandas, A. J. C. *J. Chem. Phys.* **1993**, *99*, 1076.

(20) Smith, I. W. *Kinetics and Dynamics of Elementary Gas Reactions*; Butterworths: Boston, 1980.

(21) Levine, R. D.; Bernstein, R. B. *Molecular Reaction Dynamics and Chemical Reactivity*; Oxford University Press: New York, 1987.

(22) Varandas, A. J. C. *J. Mol. Struct. (THEOCHEM)* **1988**, *166*, 59.

(23) Langhoff, S. R.; Jaffe, R. L. *J. Chem. Phys.* **1979**, *71*, 1475.

(24) Johnson, B. R.; Winter, N. W. *J. Chem. Phys.* **1977**, *66*, 4116.

(25) Peeters, J.; Mahnen, G. *Symp. (Int.) Combust.* **1972**, *14*, 133.

(26) Day, M. J.; Thompson, K.; Dixon-lewis, G. *Symp. (Int.) Combust.* **1972**, *14*, 47.

(27) Burrows, J. P.; Cliff, D. I.; Harris, G. N.; Thrush, B. A.; Wilkinson, J. P. T. *Proc. R. Soc., London* **1979**, *368*, 463.

(28) Hack, W.; Preuss, A. W.; Temps, F.; Wagner, H. Gg. *Ber. Bunsen-Ges. Phys. Chem.* **1979**, *83*, 1275.

(29) Lii, R. R.; Sauer, M. C., Jr.; Gordon, S. *J. Phys. Chem.* **1980**, *84*, 817.

(30) Atkinson, R.; Baulch, D. L.; Cox, R. A.; Hampson, R. F., Jr.; Kerr, J. A.; Troe, J. *J. Phys. Chem. Ref. Data* **1992**, *21*, 1125.

(31) Varandas, A. J. C. *Chem. Phys. Lett.* **1994**, *225*, 18.